Chapter 4

Nanowires for Room-Temperature Mid-Infrared Emission

Aiyeshah Alhodaib, Yasir J. Noori,
Anthony Krier and Andrew R.J. Marshall

Additional information is available at the end of the chapter

http://dx.doi.org/10.5772/intechopen.79463

Abstract

InAs-based nanowires hold a promise to offer transformational technologies for infrared photonic applications. Site-controlled InAs nanowire growth on low-cost Si substrates offers the practical integration advantages that silicon photonics benefits from. This includes the realisation of cheap photonic circuitries, light emitters and detectors that are otherwise expensive to realise with III/V material-based substrates. This chapter details the growth development of advanced faceted multi-quantum well structures within InAs nanowires using molecular beam epitaxy. We review the crystal structure for the faceted quantum wells along with an analysis of their optical emission characteristics which shows quantum confinement and localisation of the carriers on the quantum well nanostructure. This enables tuning of the emission wavelength and enhanced emission intensity up to the technologically important room-temperature operation point.

Keywords: indium arsenide, nanowires, multi-quantum wells, molecular beam epitaxy, photoluminescence, infrared photonics, silicon photonics

1. Introduction

Developments that took place in the past few decades in the semiconductor industry have allowed the realisation of III–V one-dimensional (1D) structures [1], such as nanowires (NWs), that have attracted increasing attention as promising materials for the fabrication of mid-infrared nanoscale devices [2]. III–V semiconductors NWs have many interesting physical and optical properties due to their narrow band gap [3], small electron effective mass [4], very high electron mobility [5], along with a great potential for realising nanoscale devices [1, 6, 7].

IntechOpen

© 2018 The Author(s). Licensee IntechOpen. This chapter is distributed under the terms of the Creative Commons Attribution License (http://creativecommons.org/licenses/by/3.0), which permits unrestricted use, distribution, and reproduction in any medium, provided the original work is properly cited.

In recent years, silicon photonics attracted a significant research effort because of the potential benefits of integrating optoelectronics functions within silicon (Si) CMOS electronic devices [8]. The growth of InAs nanowires on low-cost Si substrates paves the way towards low-cost infrared detection technologies [7]. The unique geometry of NWs structures offers new silicon photonics architectures for sensing to be operating in the mid-infrared spectral range [9], hence improving the control over the size [10], higher flexibility in sample processes [11, 12] and more freedom for band-gap engineering [13]. The field of InAs-based NWs growth in particular has attracted many researchers interest and have been extensively investigated in order to fabricate nanoscale devices including field-effect transistors [14], solar cells [15], sensor applications [16], lasers [12] and photodetectors [17].

Semiconductor NWs in nanotechnology can be synthesised through two main approaches, one is called top-down and the other bottom-up approaches [18]. The idea behind the top-down approach is to etch out and remove the crystal planes of the material from larger pieces which is usually already present on the substrate to form the nanowires. This approach mostly dominates in industry for large-scale fabrication. Few researches demonstrated successful production of NWs using this approach, for example, using InP and InGaAsP/InP materials [11, 19]. To the best of our knowledge, until today, there has not been any report of InAsSb fabricated using top-down approach; this approach shows to some extent the ability to be producing NWs for some III–V materials. However, this method suffers from drawbacks such as wire surface contamination or damages after etching treatment which hinders achieving an optimum optical performance. In the bottom-up approach, the nanostructures are built up on the substrate by adding atoms layer by layer in an ordered manner, offering the growth of a very high uniformity to the crystal structures, with a higher relative controllability in the NWs growth rate. There are two methods within the bottom-up fabrication of nanowire growth techniques: the template directed and the free-standing methods. Most of the reported NWs have been fabricated using the second approach by random or site-controlled growth.

The NWs growth mechanisms are usually governed by the famous vapour-liquid-solid (VLS) [20] or vapour solid (VS) mechanisms [21]. In the VLS approach, metal droplets are deposited on the growth substrate either through self-induced (e.g. In for InAs) or foreign metal catalyst (such as Au droplets) followed by subsequent nanowire synthesis. In the VS growth mechanism, the material starts in a vapour form inside the growth chamber and then the layers are deposited on top of the substrate epitaxially layer by layer in the solid phase, and such processes can be lithographically patterned or self-assembled. In the case of self-assembled, the NWs are grown randomly on the surface and have a variation of diameter and length. However, this kind of growth may lead to an unintentional kinking in the grown NWs [14]. Thus, controlling over position and size (diameter and length) of the NWs are required to fabricate efficient nanowire-based devices, hence allowing their applications to be realised at a large scale.

As more progress is made towards realising efficient optoelectronic devices, many methods are adapted for NWs growth, such as pulsed laser deposition [22], chemical beam epitaxy [23], metal organic chemical vapour deposition MOCVD [24] and molecular beam epitaxy (MBE) [25]. The most popular methods to grow NWs are (MOCVD) [26] and (MBE) [27]. MOCVD system and related gas phase techniques are used in the production of commercial

large-scale product, due to their high surface diffusion, fast growth rates and high throughput [28]. However, in comparison to MOCVD, solid-source MBE offers several advantages in low impurity incorporation due to the ultrahigh vacuum growth environment and the highly pure elemental growth species [26], the very accurate control over the composition of the deposited monolayer and their doping, and finally the ability to grow advanced radial and axial core-shell heterostructures via sophisticated in situ growth-monitoring methods [29].

The focus in earliest studies was on optimising the growth conditions, analyse or control the crystal structure for such wires. However, the crystal phase is particularly relevant to PL studies because the band gap and hence emission wavelength are phase dependent. In general, bulk InAs grown by conventional epitaxial techniques have a zinc-blende phase, hence its band gap ($Eg_{InAs\ (ZB)}$) is well characterised at 0.415 eV. However, by contrast, a consensus has not yet been reached around a single band gap for Wurtzite InAs ($Eg_{InAs\ (Wz)}$). While low-temperature studies build initial understanding, only a few optical emission studies have been reported, due to the very poor optical efficiency of these materials, very strong non-radiative surface and difficulties of performing spectroscopy in the IR spectral region [30]. For instance, the first low-temperature PL of InAs NWs was reported by Sun et al. [30] for InAs NWs on Si having both pure WZ and ZB crystal phases, with band energy (0.41–0.425 eV) corresponding to the above band edge surface state-related recombination, with a slight shift at increasing the temperature. They also noticed a blue shift due to quantum confinement depending on the wire diameter and not on the structure changes. Furthermore, Trägårdh et al. [31] predicted a WZ band gap of 0.54 eV from extrapolation-fitted photocurrent measurements at 5 K on single InAs NWs with a centrally placed $InAs_{1-x}P_x$ segment of the composition $0.14 < x < 0.48$. Möller et al. [32] reported temperature-dependent PL studies that enable them to estimate the wurtzite band gap to be 0.458 eV at low temperatures. Koblmuller et al. [11] have gone further to report PL temperature dependence of InAs NWs having a WZ phase structure and a peak position 0.411 eV at 15 K. Despite the strong PL emission at low temperatures, the emission was only reached 130 K before the signal was quenched [31]. The wires show a 25-meV blue shift due to confinement by reducing the wire diameters from 100 to 40 nm with respect to bulk InAs due to quantum confinement and dominant surface effect which limits PL efficiencies. The non-radiative recombination causing this quenching could originate from lattice defects, surface states or Auger recombination [31]. Recently, Rota et al. [33] estimated the energy gap for InAs WZ nanowires to be 0.477 eV, higher than the ZB band gap by 59 meV which does not depend on the nanowires size and carrier confinement. The spread of results that ranges from 0.41 to 0.54 eV may originate from polytypism, with a further complication being atmospheric absorption in the commensurate spectral range. However, while low-temperature PL measurements have supported initial studies confirming the crystal structure, emission at room temperature will be required for most practical applications. A common route to suppressing non-radiative recombination at the surfaces is the in situ growth of a wider band-gap shell which has been employed to InAs wires by Treu et al. [34] using an InAsP shell where they demonstrated 10^2 times enhancement of the PL emission up to room temperature [35]. Also, GaAs/AlGaAs core-shell NWs showed improved PL intensity compared to bulk GaAs NWs caused by the reduction in the surface states, which was found to be effective in enhancing the PL emission intensity, allowing it to persist up to room temperature. In addition to suppressing

loss through non-radiative recombination, PL intensities and quenching temperatures can be increased by acting to raise the radiative recombination rate. In a very recent study, Jurczak et al. demonstrated a 10-fold enhancement of InAs NWs PL emission using an InP core-shell layer that passivates the surface states to reduce the rate of non-radiative recombination [35]. This research direction is attracting many researchers today in order to develop advanced optoelectronic devices and nanoscale photonic applications [13]. Progress in this direction will provide further insight into the optical emission and energy band-gap properties, hence improving the use of these materials, especially for infrared detectors and emitters. This chapter discusses the concept of developing novel InAsSb/InAs multi-quantum wells (MQWs) NWs on Si (111) substrate structures within InAs nanowires, as significant step towards viable nano- and quantum emitters in the extended IR wavelength range. We review the growth process for these structures, the crystal structural characterisation. Finally, we discuss their optical properties along with developing a band structure for the NWs of this material.

2. The growth

The growth of high-quality nanowires should be achieved by avoiding the common growth process that employs a foreign catalyst such as gold to nucleate the wires. Au is well known to introduce deep level traps in the material band gap as contaminations [36, 37], which then limits the performance of the devices functionality on Si. Therefore, using lithographically predefined SiO_2 template is an additional benefit besides avoiding catalysts which enables an accurate control over positions and diameters of the grown NWs that determines where the growth occurs and allows homogeneous arrays by controlling the nucleation position without any catalysts by the selective area epitaxy technique.

In this work, the selective area molecular beam epitaxy (SA-MBE) technique has been used as a first step to grow the InAsSb/InAs MQWs NWs on Si (111) wafers and was achieved with nano-hole patterns produced by EBL [38]. The substrate is masked with a patterned dielectric layer, normally a SiO_2 layer with a thickness below 100 nm. The NW growth starts when the As and In adatoms start to form critical nuclei of certain sizes on the surface inside the patterned holes.

The MQW nanowire growth was initiated by impinging As flux followed by exposure of the sample to the In flux 20 s later. After the growth of an initial pure InAs section for 1 h, the MQW active region was grown as 10 repeats of InAs/$InAs_{1-x}Sb_x$ MQWs with growth durations of 180 and 27 s, respectively. This was expected to form 10 repeats of 25 nm InAs and 8 nm $InAs_{1-x}Sb_x$, giving a total active region thickness of 330 nm as shown in **Figure 1(a)**.

Finally, the wires were finished with an InAs cap, grown for 10 min. All growths began with a pure InAs section and were finished with an InAs cap. For further comparison, a planar bulk InAs sample was grown as a reference under the same growth conditions. The MQW NWs were grown in arrays of 50-nm diameter holes patterned using e-beam lithography in a 330-nm pitch square array defined within a number of 200 × 200 μm areas, on each silicon

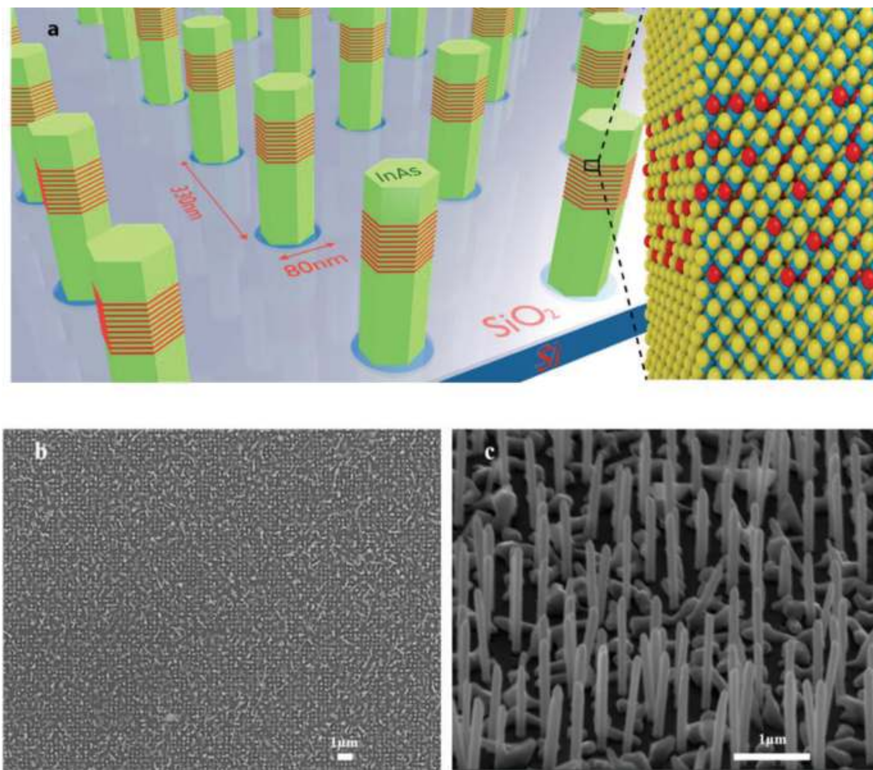

Figure 1. Nanowire structural design and analysis. (a) Schematic drawing of the InAsSb/InAs MQW within InAs NWs, grown in a 330-nm pitch square array patterned on a silicon substrate using a SiO_2 template with 80-nm diameter holes. Blue and yellow spheres represent In and As atoms, respectively, while red spheres indicate the random incorporation of Sb within the quantum well region. (b and c) Top view and tilted view SEM images, respectively. The nanowires are viewed at an angle of 70°. The scale bars in (b) and (c) are 1 μm. Figure obtained with permission from authors [38].

substrate, and the final hole diameter was ~80 nm due to lateral etching. From the SEM images, the MQW wires were on average ~1.5 μm in length and ~100 nm in diameter, see **Figure 1(b)** and **(c)**.

3. Structural analysis

The lattice structure of the InAs/InAsSb MQW NWs has been investigated using Scanning Transmission Electron Microscopy (STEM). A close inspection of high-resolution STEM images shows both the angled nature of the well and a continued WZ structure within the InAsSb well. **Figure 2** shows a full diameter image of the wire together with a zoomed-in view, within which the lattice structure can be discerned. From the zoomed-in view, it is clear that the structure of the InAsSb well does not change to ZB, as it would do in a pure InAsSb NW. However, in the case of the QWs, the short growth durations are insufficient to allow a flat top to form and so the WZ phase is maintained. Hence, the Sb fraction in the wells is currently best estimated at 6–7%, based on comparable bulk wires.

The nanowires had a regular hexagonal cross section with {10$\bar{1}$0} sidewalls, faceted tips and a twinned WZ crystal structure with stacking faults, which is a characteristic of InAs NWs [39, 40]. In common with other researchers, it has been found that the addition of Sb to form bulk InAsSb NWs forces a rotation in the layer stacking, leading to a predominantly ZB structure with a flat top. Bulk InAsSb NWs grown under these conditions contained 6–7% Sb, in good agreement with the earlier work that reports saturation at this concentration [33]. However, when the InAsSb growth is limited to nanoscale quantum wells, energy-dispersive X-ray (EDXS) mapping revealed preferential incorporation of the Sb on specific crystal planes. This results in the formation of novel quantum wells having faceted, flat-topped, conical shape, with open or partially closed flat tops, as shown in **Figure 3(a)**. It is noted that in other NW studies, the authors have considered nanoscale axial heterostructures as both quantum dots (QDs) [41, 42] and QWs [43–45]. The QD model is understandably favoured for lower-wire diameters; however, in light of the larger 100-nm diameter and the weak lateral conferment of the higher effective mass holes, the heterostructures described here are considered to be QWs.

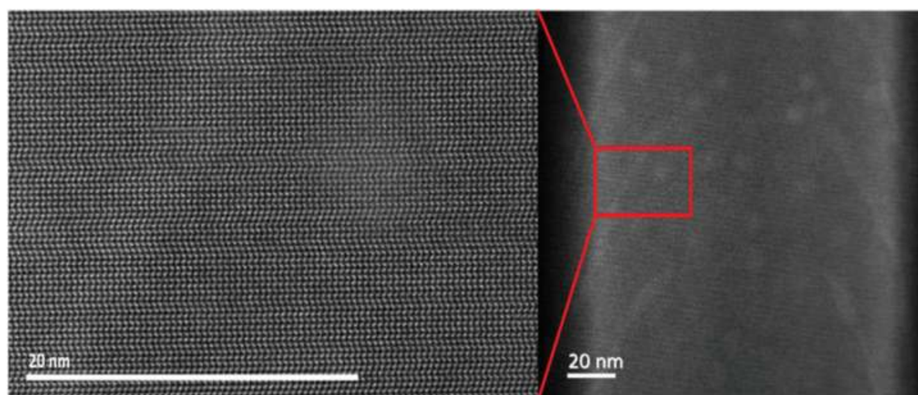

Figure 2. High-resolution TEM analysis of the QW in NW. Cross-sectional TEM images, looking across a section of wire including a QW. The lattice structure is visible, and the crystalline phase (WZ) is evidently continuous across the quantum well. Figure obtained with permission from authors [38].

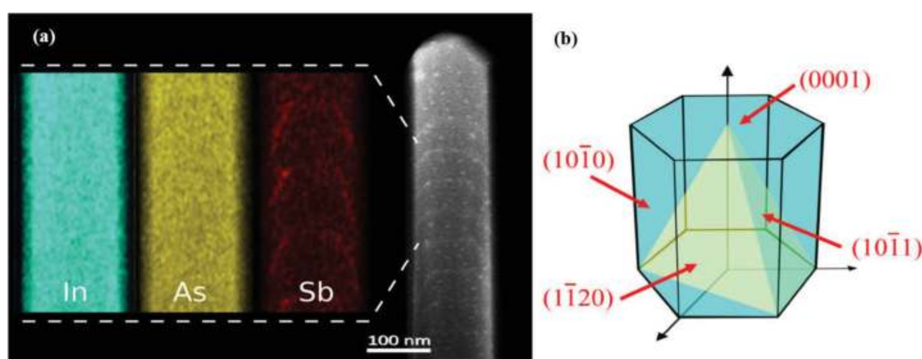

Figure 3. (a) STEM image showing the distribution of In, As and Sb obtained from 2D EDXS mapping and the resulting unusual facetted conical shape of the InAsSb MQW and (b) the unit cell of the WZ crystal structure showing the possible growth planes for the InAsSb MQW facets. Figure obtained with permission from authors [38].

4. 4-K micro-PL measurements

The 4-K PL emission from the MQW was studied using temperature-dependent micro-photoluminescence spectroscopy. Introducing the InAsSb MQW significantly changes the

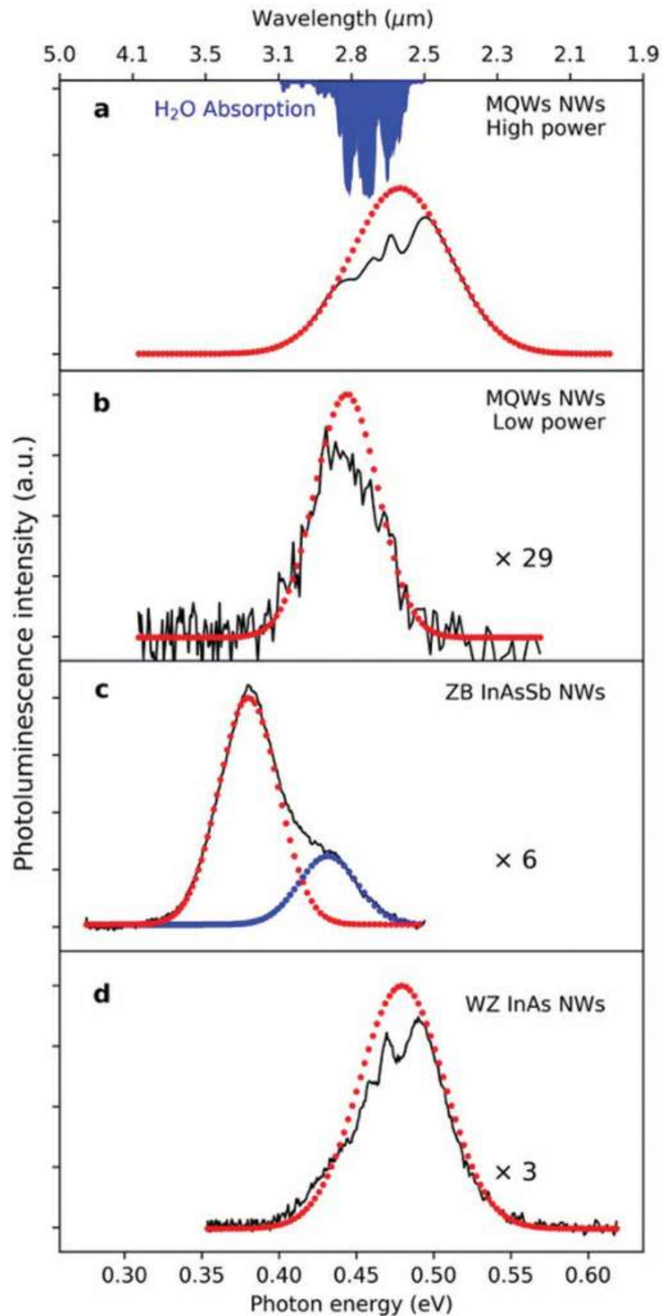

Figure 4. Micro-PL spectra obtained at 4 K. The emission spectra measured from (a) InAsSb/InAs MQW NWs at high power (1.2×10^4 W cm^{-2}), (b) InAsSb/InAs MQW NWs at low power (80 W cm^{-2}), (c) InAsSb NWs at (1.2×10^4 W cm^{-2}) and (d) InAs NWs at (1.2×10^4 W cm^{-2}). The dotted lines represent Gaussian fits to the spectra, which also reveal the atmospheric absorption from water vapour [49] in this spectral region, as shown in (a). Figure obtained with permission from authors [38].

PL emission characteristics of the NWs in a number of ways. A comparison of the spectra measured at 4 K from the InAsSb MQW NWs, bulk alloy InAsSb NWs and InAs NW samples is shown in **Figure 4**.

Figure 4(a) and **(b)** shows the PL emission from the InAsSb MQW NWs at high and low excitations, respectively. The emission from the bulk InAsSb NWs is shown in **Figure 4(c)** and are deconvoluted into peaks at 0.380 eV corresponding to 6% Sb with a dominant ZB phase in agreement with previous work [46], and a shoulder on the main peak originating from ZB InAs which appears as the dominant phase in the early stage of all the NW growths [47].

The emission from the InAs NWs peaks at 0.482 eV is shown in **Figure 4(d)**, demonstrating a dominant WZ phase [3, 33]. The PL emission of the InAsSb MQW NWs collected at high and low excitations exhibits a clear increase in peak emission energy with respect to the bulk InAsSb NWs. This is due to the strong carrier confinement within the quantum wells. In addition, the InAsSb MQW NWs also exhibit an increased emission intensity and a superior temperature-quenching behaviour compared with the bulk InAsSb NWs as expected. Most notably, the emission intensity is enhanced at all temperatures, due to the quantum confinement of electrons and holes. PL originates from type II spatially indirect recombination of electrons in the InAs layers with confined hole states in the InAsSb QWs, where the spatial separation helps in reducing non-radiative Auger recombination with a corresponding increase in radiative emission [48]. Single Gaussian fitting to the spectra reveals interference from characteristic atmospheric absorption by water vapour between 0.445 and 0.485 eV [10]. The spectra can be scaled to account for the reduced cross-sectional area of the nanowire samples, where only 7% of the surface area is covered by the NWs, assuming a 100% nucleation yield in the mask sites. Accounting for this reduced active area allows the most direct comparison of emission intensity.

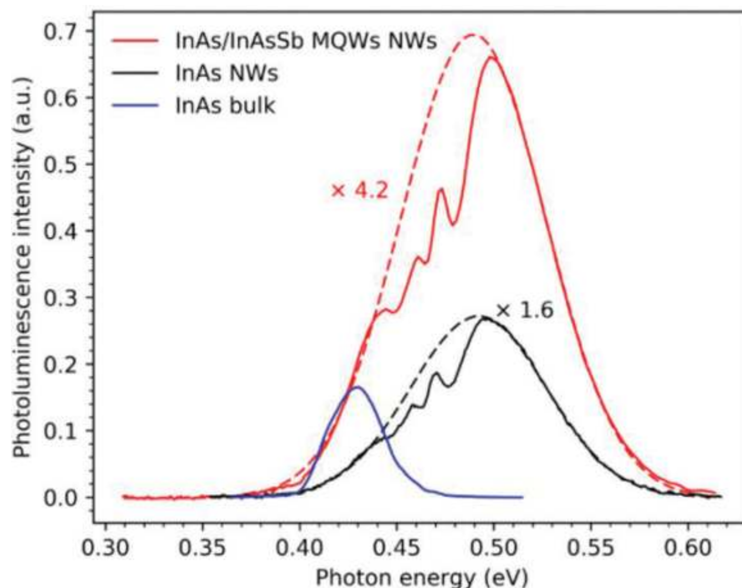

Figure 5. Comparison of emission intensities. PL spectra, under 3.2×10^4 W cm^{-2} excitation, showing the relative emission intensities for MQW NWs, InAs NWs and an InAs bulk sample, scaled by active area. Figure obtained with permission from authors [38].

We observed that at the low excitation (0.011 W cm^{-2}), the MQW NW emission intensity is 4.2-fold enhanced with respect to a bulk InAs reference sample, compared to a 1.6-fold enhancement from the InAs NWs (see **Figure 5**). It must be noted that this comparison assumes a direct area proportionality for the optical pumping efficiency. However, it has been shown that the efficiency of optical absorption in nanowire arrays exhibits a spectral dependence arising from mode guiding, due to the geometry of the wire and the array, such that the peak field can occur either inside or outside the wires [50]. To a first order, this effect is defined by the wire diameter, and in prior work, a very similar effect has been reported from an array of InAsSb NWs in a photodetector [11], where the peak response was obtained at 1.5 μm with an FWHM of 320 nm. Consequently, there is a non-optimal coupling with the 808-nm pump laser used in the present PL studies, and hence, further enhancement of PL emission intensities is to be expected if the pump laser wavelength is correctly matched to the NW geometry.

5. PL power dependence

Under low excitation conditions, bulk ZB InAs at 4 K normally exhibit characteristic emission from bound exciton and donor-acceptor transitions around 0.417 and 0.374 eV, respectively [51]. The high excitation intensity (~ 0^4 W cm^{-2}) in our micro-PL experiments results in state filling such that a single InAs peak is observed at 0.425 eV. In the present case, the InAs NW emission is further blue-shifted with respect to the bulk ZB reference sample, due to the WZ crystal structure of the NW, with a peak emission energy ranging from 0.469 eV under low excitation, to 0.485 eV under high excitation, see **Figure 6**. The band gap for WZ InAs is known to be higher than that of ZB InAs, and our result is consistent with earlier studies of WZ InAs NWs which reported band gaps in the range of 0.477–0.540 eV [12, 32].

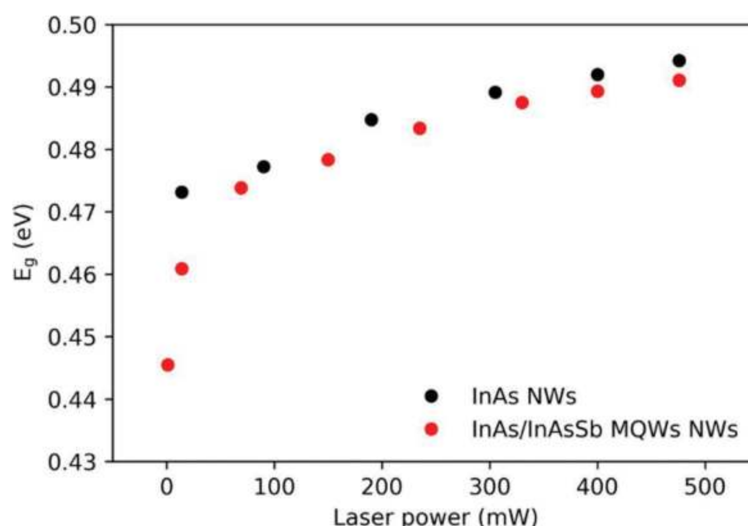

Figure 6. Power dependence of PL emission. The dependence of the peak emission energy on the power of the pump laser incident on the sample, for InAs and InAsSb/InAs MQW NWs, showing the difference in the blue shift between the pure InAs NW, with minimal quantum confinement effects and the MQW NW, with a strong quantum confinement and charging effects. Figure obtained with permission from authors [38].

Quantum confinement-induced blue shifts have also been observed as the diameter of InAs NWs is reduced [14]; however, in the case of 100-nm diameter wires, the shift is rather small ~5 meV. Hence, the emission observed from the InAs NWs grown in this work is in good agreement with earlier reports. We envisage modest size-related confinement effects in the InAsSb MQW NWs. The PL emission energy from the InAs NWs is blue-shifted by 21 meV over the range of pump powers used in our experiments, which is similar to that obtained by others [14] and is associated with band filling. The commensurate shift for the MQW NWs is much larger, at 45 meV (see **Figure 6**). The majority of this blue shift occurs at low pump powers before the dependence becomes similar to that for pure InAs wires at higher powers. The blue shift in the MQW nanowires arises due to band-bending effects characteristic of type II QWs

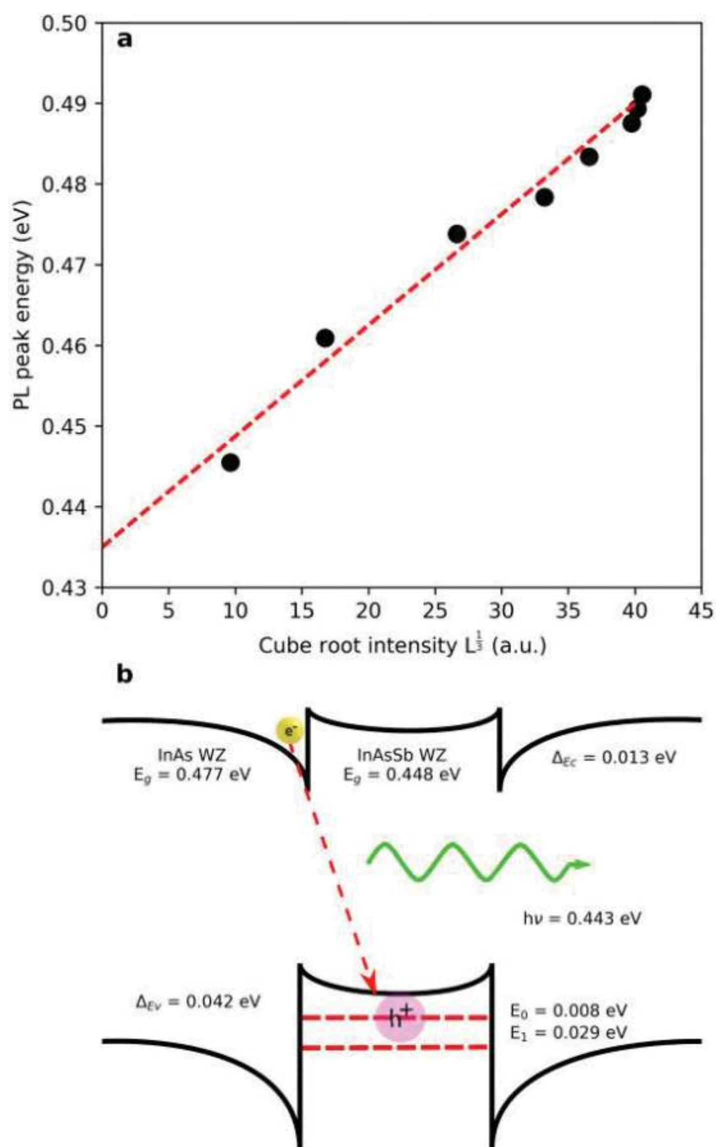

Figure 7. Determination of the flat-band transition energy at the QW. (a) PL peak energy versus cube root of integrated PL intensity, elucidating the charging of the type II QW and allowing the flat-band transition energy to be identified and (b) the calculated band diagram for the InAsSb/InAs QW and photon energy, showing the band bending and triangular well formation. Figure obtained with permission from authors [38].

http://dx.doi.org/10.5772/intechopen.79463

and originates from Coulombic attraction between localised holes in the InAsSb quantum well attracting electrons from the adjacent InAs barrier forming triangular quantum wells.

An increase in excitation intensity will raise the steepness of the confining potential and consequently the electron quantisation energy E, with a typical $\Delta E \sim L^{1/3}$ behaviour. Accordingly, the flat-band transition energy of the InAsSb/InAs MQW can be extracted from the intercept of **Figure 7(a)**—the PL peak position versus $L^{1/3}$. Consequently, the flat-band transition energy for the InAs/InAsSb MQW NWs is obtained as 0.438 eV which is in good agreement with the calculated transition energy of 0.443 eV, as shown in the schematic band diagram in **Figure 7(b)**.

6. Development of a band structure for the MQWs

Developing a band diagram for the InAs/InAsSb MQW NWs is not straightforward, due to limited data describing band gaps and alignments for the Wurtzite phases. In particular, pure $InAs_{1-x}Sb_x$ nanowires take on a predominately zinc-blende structure for x > 4%, precluding the measurement of Wurtzite band gaps at higher antimony fractions. By contrast, the $InAs_{1-x}Sb_x$ growth in this work maintains its Wurtzite structure due to the growth being on the $(10\bar{1}1)$ facets of the Wurtzite InAs wire. To approximate the band diagram in this absence of reported parameters, we start with the band alignment for a comparable zinc-blende structure, calculated taking account of the Sb fraction and the strain within a (111) orientated nanowire. The band gap of Wurtzite InAs is taken to be 60 meV greater than that for InAs zinc-blende (E_{Gwz}), with the noted caveat that there is a lack of consensus in the study. The value of the band gap for the wurtzite $InAs_{1-x}Sb_x$ can be calculated using the quadratic approximation:

$$E_g(InAs_{1-x}Sb_x) = xE_{gWZ}(InAs) + (1-x)E_{gWZ}(InSb) + x(1-x)0.67 \quad (1)$$

where 0.67 is the bowing parameter for zinc-blende InAsSb and E_{gWZ} (InSb) is the band gap of wurtzite InSb taken as 0.287 eV [52]. This gives E_g ($InAs_{0.93}Sb_{0.07}$) = 0.424 eV which is 63 meV greater than the known value for the zinc-blende phase. This also agrees with results by Farrell et al. who showed that for x = 3.9%, the band gap of Wurtzite $InAs_{1-x}Sb_x$ was also ~60 meV greater than the known value for the zinc-blende phase.

The confined hole states were calculated using a six-band k.p. solver in Nextnano. The first confined heavy hole state is calculated to be 8 meV above the band edge, as shown in the schematic energy band diagram in **Figure 7(b)** corresponding to a flat-band recombination transition energy, E_t, of 0.443 eV.

7. PL temperature dependence

PL spectra obtained at different temperatures for the InAsSb MQW NWs are shown in **Figure 8**. Although the wires are not capped or passivated, they exhibit strong PL emission which persists up to room temperature. This indicates that radiative recombination occurs primarily in the MQW away from the near surface regions, which in InAs NWs are known

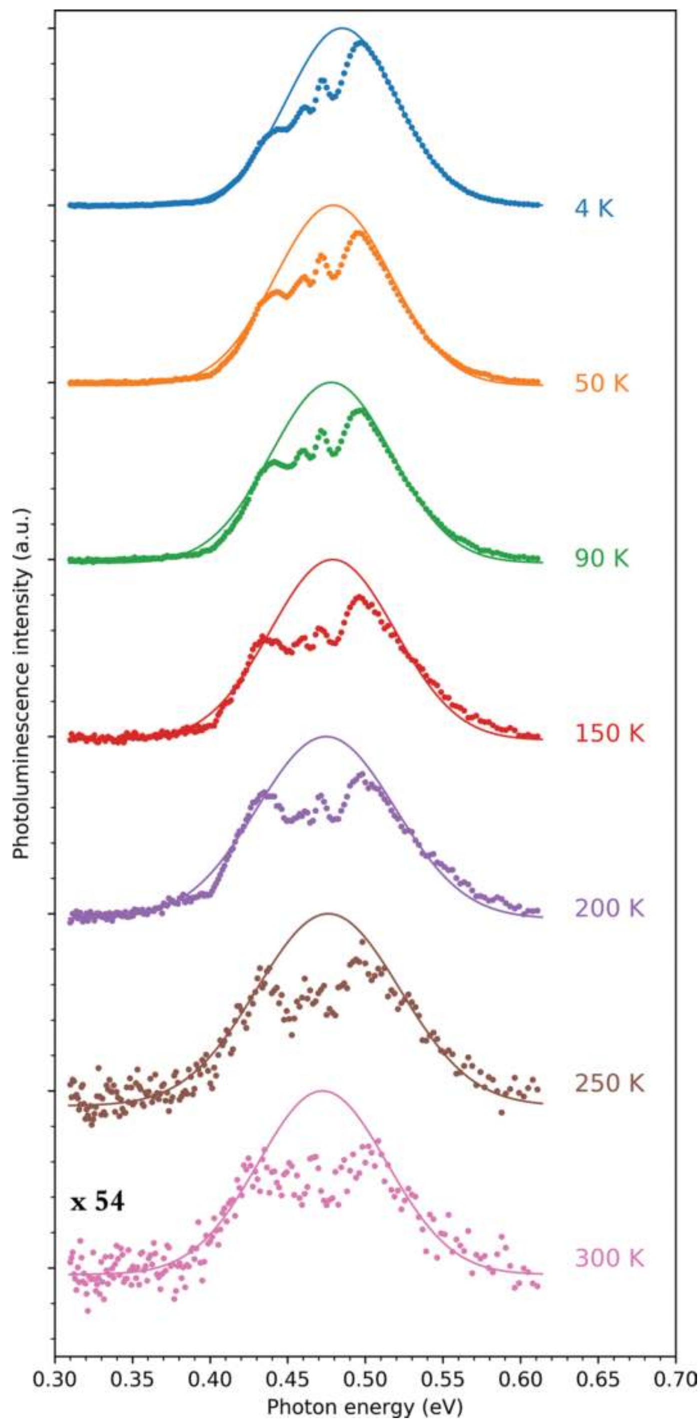

Figure 8. Temperature dependence of the PL emission spectra obtained from the InAsSb MQW NWs. Emission spectra measured over the range of 4–300 K using high excitation (2.6×10^4 W cm^{-2}), showing the room-temperature emission required for future practical NW infrared emitters. The dotted lines indicate Gaussian fits used to extract the peak emission wavelength. Atmospheric water vapour absorption is again evident in all the spectra. Figure obtained with permission from authors [38].

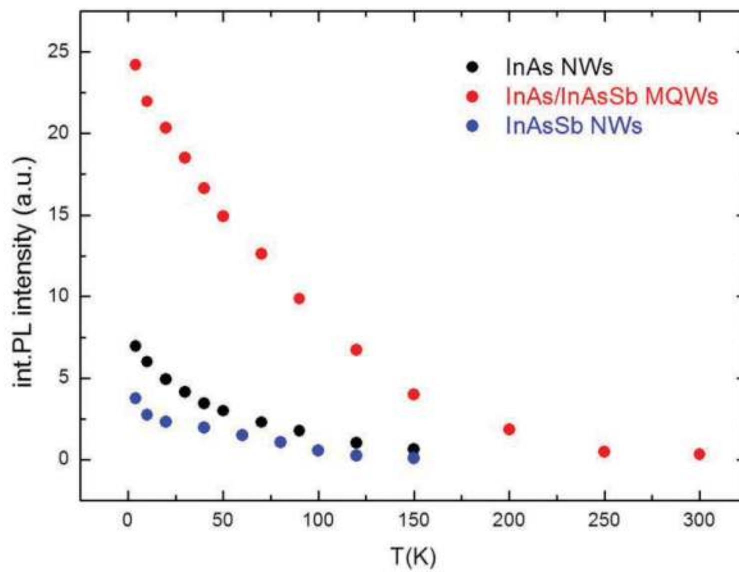

Figure 9. Temperature-dependent analysis of PL data from the InAsSb/InAs MQWs, InAsSb and InAs NW samples; the graph demonstrates quenching behaviour of the three NW sample-integrated PL intensities with increasing temperature. Figure obtained with permission from authors [38].

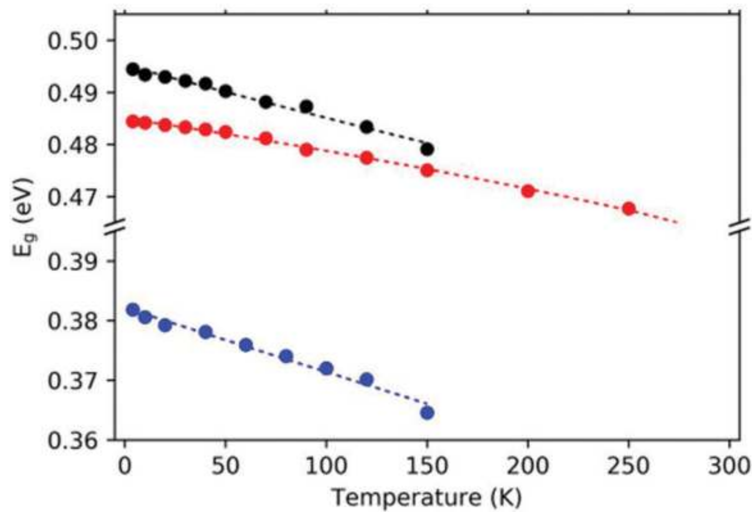

Figure 10. Temperature-dependent analysis of PL peak from the InAsSb/InAs MQWs, InAsSb and InAs NW samples. The temperature dependence of the PL peak emissions (points) was used to fit the Varshni relationships (solid lines) and extract the associated coefficients, for the three NW samples. Figure obtained with permission from authors [38].

to be accumulated due to Fermi level pinning, resulting in a low efficiency for radiative emission [53]. In our case, the quantum confinement of the MQWs allows room-temperature emission to be observed without passivation. The PL spectra are inhomogeneously broadened due to length variations in the NWs which also result in thickness variations in

the QWs. The atmospheric water vapour absorption is again evident near 2.7 μm (0.459 eV) in all the spectra.

Figure 9 presents a comparison of the temperature quenching of the NW samples, where the superior performance of the InAsSb MQW NWs is clearly evident due to the increase in the radiative emission rate and suppression of Auger recombination.

The temperature dependence of the peak energies for the NWs is shown in **Figure 10**. The dotted lines represent fitting of the results using the empirical Varshni equation. The values obtained for the fitting parameters ($E_g(0)$, α and β) are given in **Table 1** along with reference values for bulk InAs; both the InAs and the InAsSb MQW NWs have a WZ crystal structure and consequently have a weaker dependence of band gap on temperature (lower value of α) than the corresponding bulk ZB materials.

An Arrhenius plot is shown in **Figure 11** for the InAsSb MQW NWs from which an activation energy of 49 meV was obtained from the high-temperature region and ~5 meV for the low-temperature region. This is in approximate agreement with the confinement energy for thermal excitation of holes out of the QW (hole localisation energy of 34 meV) and electrons from the interface triangular QWs (<13 meV localisation energy), respectively. The activation energy of ~49 meV obtained from the Arrhenius plot is consistent with quenching due to carriers escaping confinement rather than Auger recombination and so provides indirect evidence for Auger suppression.

	E_0 (eV)	**A (meV/K)**	**β (K)**
InAs NWs	0.494	0.126	47
InAsSb NWs	0.380	0.133	42
InAsSb/InAs MQWs	0.484	0.099	97
InAs bulk	0.417	0.276	93
InSb bulk	0.235	0.320	170

Table 1. Comparison of Varshni parameters. The fitted Varshni parameters E_0, α and β for the NW samples, compared with published parameters for bulk InAs and InSb [54].

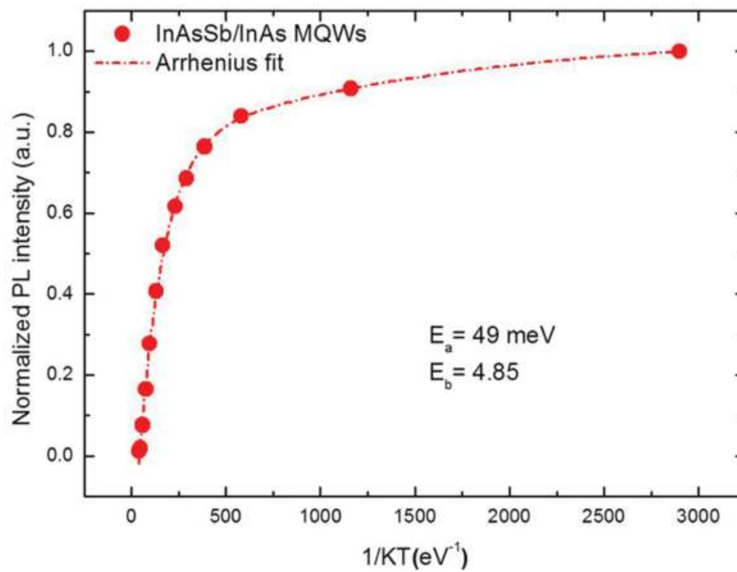

Figure 11. Temperature-dependent analysis of PL emission intensity from the InAsSb/InAs MQWs sample shows an Arrhenius plot of integrated PL intensity as a function of inverse temperature for the InAsSb/InAs MQW NWs. The curve was used to extract activation energies for the mechanisms that drive thermal quenching. Figure obtained with permission from authors [38].

In type II QWs, the Auger rate is determined by the overlap integral (between initial and final electron states at small transferred momentum) which is a minimum when the valence band offset is about three times the conduction band offset. Meanwhile, the radiative rate does not depend on the final state of any excited carrier, since it is a two-body process, so the radiative rate can remain comparable with that in a type I QW systems [55].

8. Conclusion

The development of quantum structures in NWs systems has shown the potential to extend the concept of band-gap engineering to optimise the building blocks of such systems, as well as allowing integrating these systems into the leading CMOS technology, providing a promising future for nanotechnology in optics and electronics. This chapter has presented InAsSb MQWs heterostructures within InAs NWs which exhibit mid-infrared emission at room temperature. The type II QWs provided quantum confinement and spatial localisation of the carriers combined with a suppression of Auger recombination, resulting in enhanced PL emission with respect to the bulk InAs NWs. Furthermore, having characterised the effect of charging on the type II QW, the flat-band transition energy was found to be in good agreement with calculations for both samples. These new quantum-structured NWs will allow novel nano-photonic and quantum light sources to be developed for the technologically important mid-infrared spectral range. They can exploit both the general advantages of site-controlled NWs, such as integration with silicon substrates, and also enhance light-matter coupling based on their dimensions and geometry, opening the way for a wide range of applications.

Acknowledgements

The authors gratefully acknowledge funding support for this work from the UK Centre for Defence Enterprise (Grant No. CDE65947). A.A. has been supported by a studentship funded by the Qassim University in Saudi Arabia. A.R.J.M. has been supported by individual research fellowships from the Royal Academy of Engineering.

Author details

Aiyeshah Alhodaib[1,3]*, Yasir J. Noori[2], Anthony Krier[3] and Andrew R.J. Marshall[3]

*Address all correspondence to: a3isha7@hotmail.com

1 Department of Physics, Qassim University, Buryadh, Saudi Arabia

2 Electronics and Computer Science, University of Southampton, Southampton, UK

3 Department of Physics, Lancaster University, Lancaster, United Kingdom

References

[1] Tomioka K, Tanaka T, Hara S, Hiruma K, Fukui T. III-V nanowires on Si substrate: Selective-area growth and device applications. IEEE Journal of Selected Topics in Quantum Electronics. 2011;**17**:1112-1129

[2] Kittel C. Introduction to Solid State Physics. 6th ed. New York, USA: John Wiley & Sons; 2004

[3] Pankove JI. Optical Processes in Semiconductors. Dover Books on Physics. New York: Dover Publications; 1971

[4] Hafaiedh A, Bouarissa N. Quantum confinement effects on energy GaPs and electron and hole effective masses of quantum well AlN. Physica E: Low-dimensional Systems and Nanostructures. 2011;**43**:1638-1641

[5] Joyce H, Docherty C, Gao Q, Tan H, Jagadish C, Lloyd-Hughes J, Herz L, Johnston M. Electronic properties of GaAs, InAs and InP nanowires studied by terahertz spectroscopy. Nanotechnology. 2013;**24**:214006

[6] Fukuda M. Optical semiconductor devices. New York: John Wiley & Sons; 1999. p. 7

[7] Yariv A, Yeh P. Photonics: Optical Electronics in Modern Communications. 6th ed. Oxford University Press; 2007. p. 678

[8] Reed GT, Knights AP. Silicon Photonics: An Introduction. Chichester, West Sussex, England: John Wiley & Sons Ltd; 2005

[9] Schubert EF. Physical Foundations of Solid-State Devices. Troy, New York: Rensselaer Polytechnic Institute; 2009

[10] Koblmüller G, Vizbaras K, Hertenberger S, Bolte S, Rudolph D, Becker J, Döblinger M, Amann M, Finley J, Abstreiter G. Diameter dependent optical emission properties of In: As nanowires grown on Si. Applied Physics Letters. 2012;**101**:053103

[11] Naureen S, Sanatinia R, Shahid N, Anand S. High optical quality InP-based nanopillars fabricated by a top-down approach. Nano Letters. 2011;**11**:4805-4811

[12] Thelander C, Björk M, Larsson M, Hansen A, Wallenberg L, Samuelson L. Electron transport in InAs nanowires and heterostructure nanowire devices. Solid State Communications. 2004;**131**:573-579

[13] Wang B, Leu PW. Tunable and selective resonant absorption in vertical nanowires. Optics Letters. 2012;**37**(18):3756-3758

[14] Yi G. Semiconductor Nanostructures for Optoelectronic Devices. Berlin: Springer Berlin; 2014

[15] Foldyna M, Yu L, Roca i, Cabarrocas P. Theoretical shortcircuit current density for different geometries and organizations of silicon nanowires in solar cells. Solar Energy Materials & Solar Cells. 2013;**117**:645-651

[16] Du J, Liang D, Tang H, Gao X. InAs nanowire transistors as gas sensor and the response mechanism. Nano Letters. 2009;**9**:4348-4351

[17] Miao J, Hu W, Guo N, Lu Z, Zou X, Liao L, Shi S, Chen P, Fan Z, Ho J, et al. Single InAs nanowire room-temperature near-infrared photodetectors. ACS Nano. 2014;**8**:3628-3635

[18] Hobbs R, Petkov N, Holmes J. Semiconductor nanowire fabrication by bottom-up and top-down paradigms. Chemistry of Materials. 2012;**24**:1975-1991

[19] Wang H, Sun M, Ding K, Hill M, Ning C. A top-down approach to fabrication of high quality vertical heterostructure nanowire arrays. Nano Letters. 2011;**11**:1646-1650

[20] Koto M. Thermodynamics and kinetics of the growth mechanism of vapor–liquid–solid grown nanowires. Journal of Crystal Growth. 2015;**424**:49-54

[21] Mousavi S, Haratizadeh H, Minaee H. Comparison of structural and photoluminescence properties of zinc oxide nanowires grown by vapor–solid and vapor–liquid–solid methods. Thin Solid Films. 2012;**520**:4642-4645

[22] Obi D, Nechache R, Harnagea C, Rosei F. Mechanical and electrical properties of epitaxial Si nanowires grown by pulsed laser deposition. Journal of Physics: Condensed Matter. 2012;**24**:445008

[23] Radhakrishnan G, Freundlich A, Charlson J, Fuhrmann B. III-V semiconductor vertical and tilted nanowires on silicon using chemical beam epitaxy. MRS Proceedings. 2007;**1031**:H13-01

[24] Dayeh SA, Yu ET, Wang D. Growth of InAs nanowires on SiO_2 substrates: Nucleation, evolution, and the role of Au nanoparticles. Journal of Physical Chemistry C. 2007;**111**:13331

[25] Tchernycheva M, Travers L, Patriarche G, Glas F, Harmand JC, Cirlin GE, Dubrovskii VG. Au-assisted molecular beam epitaxy of InAs nanowires: Growth and theoretical analysis. Journal of Applied Physics. 2007;**102**:094313

[26] Zhang X, Zou J, Paladugu M, Guo Y, Wang Y, Kim Y, Joyce HJ, Gao Q, Tan HH, Jagadish C. Evolution of epitaxial InAs nanowires on GaAs (111) B. Small. 2009;**5**:366-369

[27] Ihn SG, Song JI. InAs nanowires on Si substrates grown by solid source molecular beam epitaxy. Nanotechnology. 2007;**18**:355603

[28] Henini M. Molecular Beam Epitaxy. Burlington: Elsevier Science; 2013

[29] Ashok S. Defect and Impurity Engineered Semiconductors and Devices III. Warrendale, Pa: Materials Research Society; 2002

[30] Sun M, Leong E, Chin A, Ning C, Cirlin G, Samsonenko Y, Dubrovskii V, Chuang L, Chang-Hasnain C. Photoluminescence properties of InAs nanowires grown on GaAs and Si substrates. Nanotechnology. 2010;**21**:335705

[31] Trägårdh J, Persson A, Wagner J, Hessman D, Samuelson L. Measurements of the band gap of Wurtzite $InAs_{1-X}P_X$ nanowires using photocurrent spectroscopy. Journal of Applied Physics. 2007;**101**:123701

[32] Möller M, de Lima M Jr, Cantarero A, Chiaramonte T, Cotta M, Iikawa F. Optical emission of InAs nanowires. Nanotechnology. 2012;**23**:375704

[33] Rota M, Ameruddin A, Fonseka H, Gao Q, Mura F, Polimeni A, Miriametro A, Tan H, Jagadish C, Capizzi M. Bandgap energy of wurtzite InAs nanowires. Nano Letters. 2016;**16**:5197-5203

[34] Treu J, Bormann M, Schmeiduch H, Döblinger M, Morkötter S, Matich S, Wiecha P, Saller K, Mayer B, Bichler M, et al. Enhanced luminescence properties of InAs–InAsP core–shell nanowires. Nano Letters. 2013;**13**:6070-6077

[35] Jurczak P, Zhang Y, Wu J, Sanchez A, Aagesen M, Liu H. Ten-fold enhancement of InAs nanowire photoluminescence emission with an InP passivation layer. Nano Letters. 2017;**17**:3629-3633

[36] Sourribes MJL, Isakov I, Panfilova M, Liu H, Warburton PA. Mobility enhancement by Sb-mediated minimisation of stacking fault density in InAs nanowires grown on silicon. Nano Letters. 2014;**14**:1643-1650. PMID: 24502770

[37] Brotherton SD, Lowther JE. Electron and hole capture at Au and Pt centers in silicon. Physical Review Letters. 1980;**44**:606-609

[38] Alhodaib A, Noori Y, Carrington P, Sanchez A, Thompson M, Young R, Krier A, Marshall A. Room-temperature mid-infrared emission from faceted InAsSb multi quantum wells embedded in InAs nanowires. Nano Letters. 2017;**18**:235-240

[39] Johansson J, Bolinsson J, Ek M, Caroff P, Dick KA. Combinatorial approaches to understanding polytypism in IIIV nanowires. ACS Nano. 2012;**6**:6142-6149. PMID: 22681568

[40] Dick K, Thelander C, Samuelson L, Caroff P. Crystal phase engineering in single InAs nanowires. Nano Letters. 2010;**10**:3494-3499

[41] Wu J, Ramsay A, Sanchez A, Zhang Y, Kim D, Brossard F, Hu X, Benamara M, Ware M, Mazur Y, et al. Defect-free self-catalyzed GaAs/GaAsP nanowire quantum dots grown on silicon substrate. Nano Letters. 2015;**16**:504-511

[42] Reimer M, Bulgarini G, Akopian N, Hocevar M, Bavinck M, Verheijen M, Bakkers E, Kouwenhoven L, Zwiller V. Bright single-photon sources in bottom-up tailored nanowires. Nature Communications. 2012;**3**:737

[43] Yang L, Motohisa J, Takeda J, Tomioka K, Fukui T. Size-dependent photoluminescence of hexagonal nanopillars with single InGaAs/GaAs quantum wells fabricated by selective-area metal organic vapor phase epitaxy. Applied Physics Letters. 2006;**89**:203110

[44] Ra Y, Navamathavan R, Park J, Lee C. High-quality uniaxial InxGa1–XN/GaN multiple quantum well (MQW) nanowires (NWs) on Si (111) grown by metal-organic chemical vapor deposition (MOCVD) and light-emitting diode (LED) fabrication. ACS Applied Materials & Interfaces. 2013;**5**:2111-2117

[45] Armitage R, Tsubaki K. Multicolour luminescence from InGaN quantum wells grown over GaN nanowire arrays by molecular-beam epitaxy. Nanotechnology. 2010;**21**:195202

[46] Farrell A, Lee W, Senanayake P, Haddad M, Prikhodko S, Huffaker D. High-quality InAsSb nanowires grown by catalyst-free selective-area metal–organic chemical vapor deposition. Nano Letters. 2015;**15**:6614-6619

[47] Thompson M, Alhodaib A, Craig A, Robson A, Aziz A, Krier A, Svensson J, Wernersson L, Sanchez A, Marshall A. Low leakage-current InAsSb nanowire photodetectors on silicon. Nano Letters. 2016;**16**:182-187

[48] Carrington P, Zhuang Q, Yin M, Krier A. Temperature dependence of mid-infrared electroluminescence in type II InAsSb/InAs multi-quantum well light-emitting diodes. Semiconductor Science and Technology. 2009;**24**:075001

[49] Lord SD. NASA Tech. Memo. 103957. 1992

[50] Svensson J, Anttu N, Vainorius N, Borg B, Wernersson L. Diameter-dependent photocurrent in InAsSb nanowire infrared photodetectors. Nano Letters. 2013;**13**:1380-1385

[51] Heber JD, Philips CC. InAs/InAsSb emitters for the mid-infrared region. In: Cai WZ. III-V Semiconductor Heterostructures: Physics and Devices. Keraia: Research Signpost; 2003. pp. 140-167

[52] De A, Craig E. Predicted band structures of III-V semiconductors in the wurtzite phase. Physical Review B. 2011;**84**:239907

[53] Olsson L, Andersson C, Håkansson M, Kanski J, Ilver L, Karlsson U. Charge accumulation at InAs surfaces. Physical Review Letters. 1996;**76**:3626-3629

[54] Latkowska M et al. Temperature dependence of photoluminescence from InNAsSb layers: The role of localized and free carrier emission in determination of temperature dependence of energy gap. Applied Physics Letters. 2013;**102**:122109

[55] Zegrya GG, Andreev AD. Mechanism of suppression of Auger recombination processes in type II heterostructures. Applied Physics Letters. 1995;**67**(18):2681